Compressive Sensing Applied to Planar Near-Field Based Array Antenna Diagnostics for Production Testing

C.G. Parini[1],
(1) Queen Mary University of London,
London, Mile End Road,
E1 4NS, UK

S.F. Gregson[1,2]
(2) Next Phase Measurements,
11521 Monarch St, Garden Grove,
CA, USA

Abstract*—Compressive Sensing (CS) has been deployed in a variety of fields including wideband spectrum sensing, active user detection and antenna arrays. In massive MIMO arrays, CS has been applied to reduce the number of measurements required to verify the arrays excitation in a production environment. All follow the general approach of creating the sparsity needed for CS by subtracting the measured far-field or near-field of the test array from that of a 'gold standard' array measured under identical conditions. In a previous paper [1] the authors have shown that using a Far-Field Multi-Probe Anechoic Chamber (FF-MPAC) and an optimal sampling strategy CS can offer accurate reconstruction of array excitation with a mean square error (MSE) approaching -40dB using a sampling strategy of just 1.4% of the Nyquist rate. The approach assumed production standard arrays with failure rates up to around 2%. In this paper we extend the concept to using a planar near-field (NF) measurement offering a much more compact test facility that is more suited to the production environment for these antennas. In our initial work the reconstruction of array excitation with a mean square error (MSE) of -30dB was achieved for a 20 x 28 element array antenna at half wavelength spacing using just 1.5% (177 samples) of the samples needed for a conventional NF measurement (12,100 samples) employing back projection to the aperture. Critical to the performance is the realization that the CS samples need to be confined to the central region of the NF measurement plane which for a conventional NF to FF planar antenna pattern measurement would offer a massive truncation error. This paper addresses the optimal sampling strategy needed for this NF approach and presents a statistical performance analysis of the reconstruction accuracy.

I. INTRODUCTION

The 5th generation new radio (5GNR) promises many new possibilities, however, perhaps the circa ten-to-twenty-fold increase in data rate is the most significant to the antennas and propagation community as this has necessitated the adoption of several important new technologies. Chief amongst these is the move to higher frequency bands, and the adoption of far more complex Massive MIMO (Multiple Input Multiple Output) array antenna architectures and electronic beam scanning, which are needed to handle the associated increase in free-space RF path-loss. Although the frequency band below 6 GHz may be used during the initial rollout, 5G technologies will mainly occupy the 28 GHz, RF2, frequency band, or possibly higher, necessitating the widespread use of more complex, electrically larger, massive MIMO antennas [2, 3]. With the adoption of these more complex phased array antennas (typically comprising many thousands of elements), comes the need to test and calibrate them as part of the production process. Generally, techniques developed for high value, low volume production, arrays used in space and aerospace applications are time consuming and inappropriate for mass manufacture. Such techniques include using a single low Radar Cross Section (RCS) probe to measure the field close to each array aperture, or the use of Near-Field/Far-Field (NF/FF) measurements to verify the FF beam or back project into the aperture to verify element excitations [4]. For volume production of massive MIMO arrays such studies need to be undertaken at the development stage leading to the creation of a reference or 'gold' standard antenna which then needs to be replicated in volume. Thus, we need to consider alternative methods to drastically reduce the number of measurements and the time needed to determine an arrays excitation by making use of the known excitations of the 'gold' antenna.

Compressive Sensing (CS) has been deployed in a range of disciplines and works on the principle that we can reconstruct a big space (P), from just a few samples (S) providing we can find an appropriate transform that enables the big space to be defined by only a few variables within this sparse domain. For the case of antennas, an array of sources can be used to define the whole of the far-field radiation pattern in the forward half-space using the plane wave spectrum or the equivalent sources method. When using the equivalent sources method, the inverse transform from the NF to aperture is the 'compressed sensing' protocol with the key to compressive sensing being recovering the full measurement from the compressed ones by utilizing the sparsity property [5] from a few scattered measurements.

CS was first applied to the spherical near-field (SNF) case to reduce the number of NF measurements needed by exploiting the inherent sparsity property of spherical mode coefficients (SMCs) [6, 7] and hence shorten the acquisition time with a smaller number of NF measurements and so increasing measurement speed. The developed sampling schemes have also been applied to non-spherical geometries,

with CS being successfully utilized to reduce the truncation error in cylindrical NF measurements [8].

Alternatively, [9-11] presented the idea of applying CS to array diagnosis from either NF or FF measurements. Here, instead of attempting to reduce the number of measurement points required for NF to FF transformation, they assume that the number of failed elements was much smaller than the total number of elements within the array and this was a critical step to providing the requisite sparsity property. This technique requires the availability of a 'gold' antenna and imposes upper bound limits on the amount of measurement noise permissible if the reconstruction of a given number of faults is to be successfully determined.

In this paper, we exploit the fact that the 'gold' reference antenna exists, and explore the use of CS to undertake a back transform to the array aperture from the PNF measurement of the difference between the NF pattern of the AUT, and the 'gold' antenna using minimal, randomly located, radiated NF samples. Here, the aim is to minimise the number of measurement points required to reliably and accurately measure the antenna in the NF, whilst accurately reconstructing the array element excitations. The approach used in this paper is summarized in Fig. 1, where the back projected aperture field indicates just the difference between the aperture field of the "defective" production antenna, and the 'gold' reference antenna.

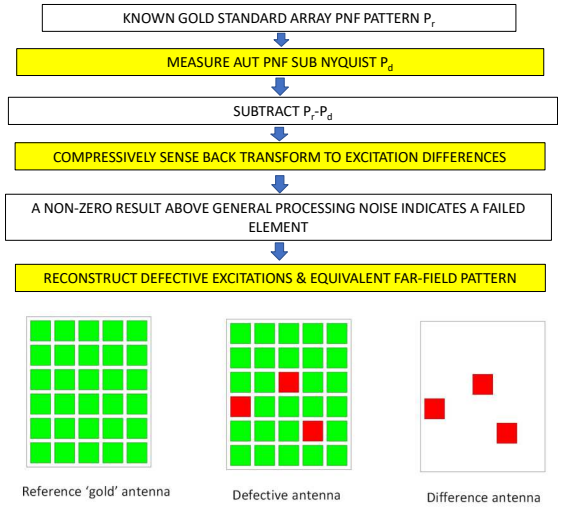

Figure 1. Top: Flow diagram of defective element detection using compressive sensing. Bottom: the 'sparse' difference antenna concept.

II. Equivalent Currents Method

The equivalent magnetic current approach we use here utilises conventional planar near-field data to obtain an equivalent magnetic current sheet over a convenient surface that encloses the AUT which can then be used to obtain the desired electric fields elsewhere in space including the far-field [12]. In this procedure, an electric field integral equation is derived which relates the measured near-field to the equivalent magnetic currents which is solved using an efficient, all be it resource intensive, moment method procedure [12], with point matching which converts the integral equation into an equivalent matrix-equation which can be solved in one of a number of ways, *e.g.* by using the least squares conjugate gradient (LSQR) method [13].

Let us assume that the antenna is placed in one half-space, and is radiating into the other, forward half-space, with an infinite *xy*-plane dividing the two regions. If an infinite electric conducting sheet is postulated on one side of the surface, then in this case only the tangential components of the electric fields need be specified on the surface. The magnetic current is then provided by [12],

$$\underline{J}_m(\underline{r}') = \begin{cases} 2\left(\underline{E}_a(\underline{r}')\times\hat{\underline{n}}\right) & \text{over the aperture} \\ 0 & \text{elsewhere} \end{cases} \tag{1}$$

The radiated fields must be determined in the presence of the conducting sheet which results in the solutions only being available for the forward half-space. The electric vector potential $\underline{F}$ may be defined as [12],

$$\underline{F}(\underline{r}) = \frac{\varepsilon}{4\pi}\int_S \frac{\underline{J}_m(\underline{r}')}{R} e^{-jk_0R} ds' \tag{2}$$

Here, the free-space propagation constant is denoted by k_0, primed variables are associated with the source point, and un-primed variables are associated with the field point where the distance R can be expressed as,

$$R = |\underline{r} - \underline{r}'| = \sqrt{(x-x')^2 + (y-y')^2 + (z-z')^2} \tag{3}$$

We may obtain the electric fields from the electric vector potential $\underline{F}$ as [12],

$$\underline{E}(\underline{r}) = -\frac{1}{\varepsilon}\left(\nabla'\times\underline{F}(\underline{r}')\right) \tag{4}$$

Thus,

$$\underline{E}(\underline{r}) = \frac{1}{4\pi}\int_S \underline{J}_m(\underline{r}')\times\nabla' g(\underline{r},\underline{r}')\, ds' \tag{5}$$

Here $\underline{E}(\underline{r})$ is the field that is measured over the planar acquisition surface S located at a distance of a few wavelengths from the AUT, $\underline{J}_m$ denotes the surface magnetic current sheet that we seek. Assuming a Cartesian coordinate system and polarization basis we may write this in a more convenient form [12],

$$E_x(\underline{r}) = \frac{1}{4\pi}\int_S \frac{e^{-jk_0R}}{R^2}(z-z')\left(jk_0 + \frac{1}{R}\right) J_{my}(\underline{r}')\, ds' \tag{6}$$

$$E_y(\underline{r}) = \frac{-1}{4\pi}\int_S \frac{e^{-jk_0R}}{R^2}(z-z')\left(jk_0 + \frac{1}{R}\right) J_{mx}(\underline{r}')\, ds' \tag{7}$$

This can be solved using a method of moments approach [12]. We may now use the sampling theorem to replace the continuous electric fields with a set of discrete samples, and the current sheet with an array of fictitious magnetic dipoles. This latter assumption is equivalent to using a delta function as the expansion function for the current source within the integrand, and enables us to replace the integration with a summation which allows us to express this in an equivalent matrix form yielding,

$$[E_x] = [G][J_{my}] \tag{8}$$

$$[E_y] = -[G][J_{mx}] \tag{9}$$

The elements in the matrix [G] can be obtained by evaluating,

$$G_{k,l} = \frac{1}{4\pi} \int_{S_{k,l}} \frac{e^{-jk_0 R}}{R_{k,l}^2} (z_k - z_l') \left(jk_0 + \frac{1}{R_{k,l}} \right) ds' \tag{10}$$

If the reconstructed currents are *more* than a wavelength away from the measurement surface, then the area of integration may be collapsed to that of an infinitesimal current element. Thus, the excitation coefficients for the fictitious magnetic dipole array can be obtained by solving the system of equations [12],

$$[G]^{-1}[E_x] = [J_{my}] \tag{11}$$

$$[G]^{-1}[E_y] = -[J_{mx}] \tag{12}$$

If the number of measured near-field points equals the number of fictitious magnetic dipoles, then this system of equations may be solved uniquely. If the number of measured points is greater than the number of dipoles, *i.e.* current elements, then this may be solved in a least squares sense. Crucially, this system of equations is in a form that the CS method can be employed, with this being described in the next section.

III. Defective Element Detection Using Compressive Sensing

In this CS system, we assume the availability of the failure-free 'gold' antenna array, whose N radiating elements' excitation coefficients are defined as $X_r = \{x_1, \ldots, x_n, \ldots x_N\}^T$, where x_n is the excitation coefficients of the n^{th} radiating element. The corresponding NF pattern vector is denoted as $P_r = \{p_1, \ldots, p_m, \ldots, p_M\}^T$, where p_m is the probe voltage measured at the m^{th} NF sampling point of a total of M sample points. Correspondingly, we denote X_d as the excitations of the (defective) AUT collected at sub-Nyquist sampling rate and P_d as the probe measured NF pattern collected from the AUT. Then we consider the following system:

$$P = AX + N \tag{13}$$

where $P = P_r - P_d$, $X = X_r - X_d$, $N(0, \sigma^2)$ is additive white Gaussian noise (AWGN) with zero mean and variance σ^2 and is set by specifying a given signal-to-noise ratio for the measurement environment. Let $A = \psi U$ with the binary sampling matrix $\psi \in C^{M \times K}$ selects M rows randomly from the discrete Fourier matrix $U \in C^{K \times N}$. Note that the choice influences the recovery performance significantly, which will be discussed in the next section. The element (k, n) of the matrix U is defined as:

$$[U]_{k,n} = \frac{1}{\sqrt{N}} e^{-j2\pi \frac{kn}{N}} \tag{14}$$

where k is the number of Nyquist sample points. The task of array diagnosis is to detect the faulty elements. We denote the number of faulty elements as F, which is much smaller than the number of radiating elements N. Therefore, X is an F-sparse vector, in which only the faulty elements of the original array contribute to the sparse support. By doing so, we convert the problem into a sparse one. Compressive sensing can be applied to recover X_d with the knowledge of the excitation coefficients of the 'gold' antenna, X_r, by solving the following problem:

$$\min_X \|X\|_0 \quad s.t. \ \|P - AX\|_2 < \sigma^2 \tag{15}$$

where σ^2 is determined by the noise level affecting the measured samples P_d and P_r. It is noted that the above l_0 problem is non-convex and difficult to solve. In compressive sensing, it has been relaxed to an l_1 problem with guarantee on exact recovery when the restricted isometry property is satisfied. Therefore, the optimization problem becomes,

$$\min_X \|X\|_1 \quad s.t. \ \|P - AX\|_2^2 < \sigma^2 \tag{16}$$

Note that the above l_1 problem is convex, which could be solved by standard convex optimization tools. In this paper, we utilise the CVX toolbox [14] to solve (16). The whole procedure of compressive sensing based defective array detection can be seen summarized in Fig. 1.

It is noted the reweighted l_1 norm has been proposed in [15] to provide less penalty on the non-zero element in X. By introducing the weight to (16), the convex problem is solved in an iterative way. In the l^{th} iteration, the convex problem is solved as,

$$\arg\min \sum_{n=1}^{N} \|w_n^l x_n^l\|_1 \quad s.t. \ \|P - AX^l\|_2^2 < \sigma^2 \tag{17}$$

where $w_n^l = 1/\left(|x_n^{l-1}| + \eta\right)$ defines the weight for x_n^l, and η is a small positive constant to ensure the numerical stability of the algorithm. In general, the solution is robust to the choice of η. We note that $w_n^0 = 1$ is taken as the initial value, which makes the reweighted l_1 problem the same as the typical l_1 problem.

The above CS process can be directly applied to a one-dimensional linear array, where X_d is the recovered excitations. For the case of a two-dimensional array we simply wrap this two-dimensional array of excitations into a one-dimensional vector whilst managing the correct phase relationship between two-dimensional elements and NF radiation. Thus, for a 20 x 28 element array X_d has dimension 560, and in the following sections, we will show the application of CS to two-dimensional array diagnosis.

IV. Measurement simulations

We first consider a conventional PNF scan of a 20 x 28 element dipole array with half wavelength spacing and operating at 8.2GHz. The scan plane is 2m by 2m with the NF probe distance of 3λ from the aperture and a measurement noise level set at -60dB from the peak signal level, with NF

measurement points separated by half wavelengths (λ/2) in *x* and *y* which results in 12,100 sample points. We now add four randomly located faults to this array of the form -6dB and 45°; -10dB and -75°; -30dB and 135°; -3dB and 110° and simulate the defective NF. We can then compute a conventional vector Huygens' back transform to the array aperture and obtain the amplitude and phase excitation of the defective array as shown in Figure 2.

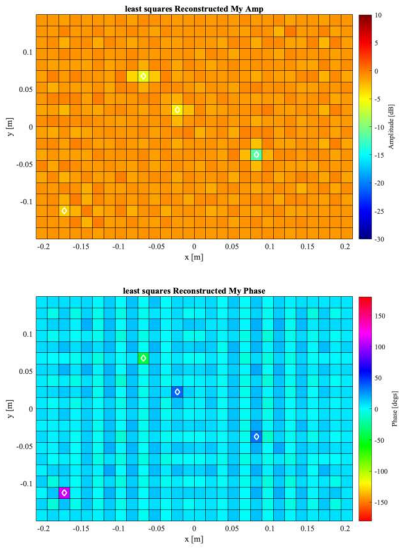

Figure 2. Back transformed array excitations for defective array. Defective elements indicated by white diamond. Top: amplitude, bottom: phase.

Considering the element excitation as a complex number the RMS element excitation error over the whole array was -15.5 dB with maximum error of -8.4 dB, this taking account of both amplitude and phase errors as a single performance parameter. The false alarm level (RMS error amplitude calculated over the elements that were not faulty) was -25.7 dB with a maximum of -11.9 dB. From these results we see that the phase errors are quite well defined, but the amplitude errors are less so, all with a considerable 'background noise' to the excitations.

We now turn our attention to using the CS diagnostic process described above which in this case takes the difference between the near-fields of the reference and defective antennas. The resulting reconstructed excitations of the defective array are shown in Figure 3. In this case the RMS element complex excitation error over the whole array was -31.7 dB with maximum error of -9.4 dB and the false alarm level was -39.9 dB with a maximum of -19.2 dB. These results are considerable better than the conventional back projection results with clearly much lower background noise (low false alarm level). Crucially this was achieved with just 177 NF samples, which is just 1.5% of the conventional back projection case of 12,100 λ/2 spaced samples.

Critical to achieving this result is the realization that the CS samples need to be confined to the *central* high intensity field region of the NF measurement plane, which is effectively the projection of the array aperture, as shown by the white rectangle in the NF phase plot of Figure 4. For a conventional NF back projection process such a data truncation would offer massive reconstruction error. In both cases, these measurement simulations were taken with each NF point being subject to -60dB of background noise.

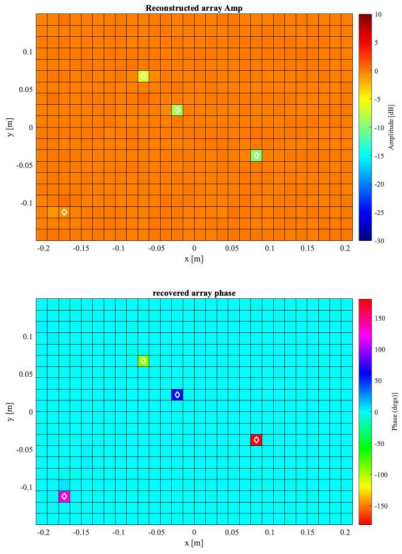

Figure 3. CS based reconstruction of array amplitude excitations for defective array. Defective elements indicated by white diamond. Top: amplitude, bottom: phase.

This result is just a snapshot, and we need to take a far broader statistical view by running a random selection of fault locations many times, and plotting the cumulative distribution function (CDF) [1] of the mean square error (MSE).

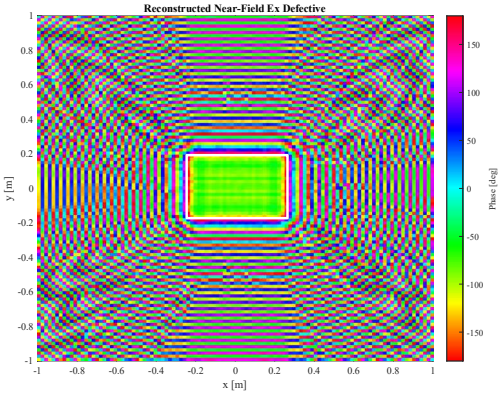

Figure 4. NF phase of defective array showing sample space as white rectangle

Figure 5 shows the CDF MSE over 50 runs in the presence of -60 dB noise. If we take the 80% CDF MSE level as a useful reference point to compare results (*i.e.* 80% of the runs will be better than or equal to this MSE value), then this result shows a MSE of -33.1 dB. We have taken the 80% CDF point rather than the one-sigma (68%) point, or the two-sigma (95%) as arguably it provides a fairer representation of system performance. Also shown on this figure is the CDF MSE of

just the faulty elements, which for this case is -12.8 dB at the 80% point. The CDF of the maximum value of the excitation error for each run is also shown in Figure 5 and at the 80% CDF point is -10 dB.

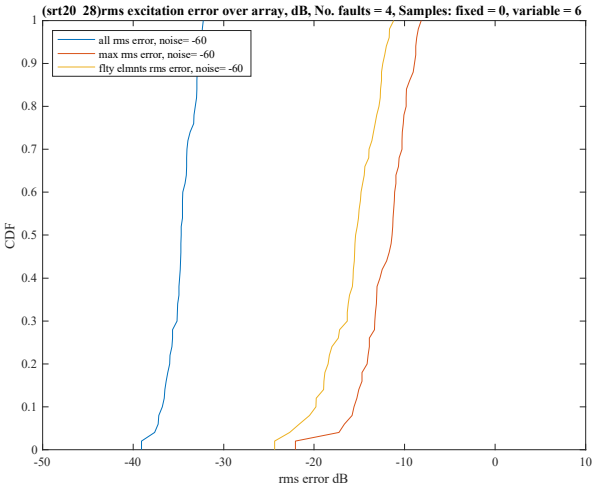

Figure 5. CDF of amplitude excitation error with statistics taken over 50 random sets of 4 fault locations. Faults fixed as shown in the inset table.

To achieve these results for a given set of 4 faults we take 36 random samples within the NF sample rectangle (shown in Figure 6) and use CVX [16] to solve equation (16). We then repeat this 'measurement' process six times with different sets of 36 sample points, applying random noise to each of the sets to simulate a true noisy measurement. The resulting six sets of reconstructed array excitations are then averaged to achieve the overall result reconstruction shown in Figure 3.

Since each set of 36 samples is pseudo-randomly selected within the sample space, and this is achived by dividing the sample space into 36 equal size rectangles and then randomly selecting on sample point within each rectangle. This process means that some samples points are used more than once (see Figure 6) and this results in the total number of unique samples being taken as 177 in the case of Figure 3.

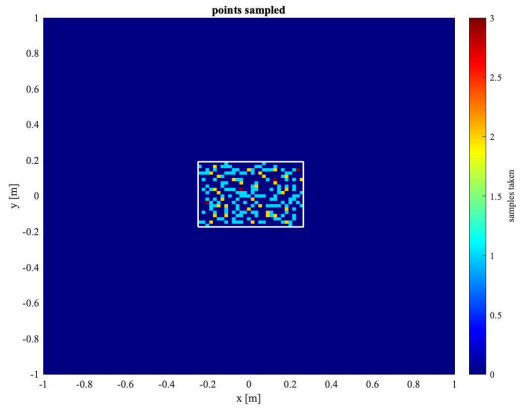

Figure 6. CS NF samples taken in optimal central NF region only, 36 random points repeated six times.

In a real-life measurement, these six sets of 36 samples can be determined a priori and so the desired unique measurement points can then be measured using a robotic arm mounted NF probe. For the case of Figure 5, where this whole process is repeated 50 times with different fault locations the average number of samples needed per reconstruction was 182.

We have rerun the results of Figure 5 with different number of the 36 sample sets, and the results are presented in Table I.

TABLE I. RECONSTRUCTION PERFORMANCE WHEN AVERAGING OVER DIFFERENT NUMBERS OF 36 SAMPLE SET RUNS. ARRAY HAS FAULTY ELEMENTS

number of runs	excitation error at 80% CDF MSE (dB)	faulty element error at 80% CDF MSE (dB)	average number of samples
1	-29.9	-11.4	36
2	-31.7	-13.3	70
4	-33.1	-13.8	131
6	-33.1	-12.8	183
6[1]	-34.9	-14.9	184
10	-34.3	-14.3	268

[1] array is beam scanned to 20° in azimuth and 10° in elevation.

For this case of 36 samples per run, averaging over 4 or 6 runs gives a good balance of performance with 4 faults. If we average over 6 runs and then look at the performance for different numbers of faulty elements, we get the results shown in Table II.

TABLE II. RECONSTRUCTION PERFORMANCE FOR DIFFERENT NUMBER OF FAULTY ELEMENTS WHEN AVERAGING OVER SIX SETS OF 36 SAMPLE RUNS

number of faulty elements	excitation error at 80% CDF MSE (dB)	faulty element error at 80% CDF MSE (dB)	average number of samples
2	-39.2	-17.4	184
4	-33.1	-12.8	183
6	-33.6	-16.9	183
8	-28.7	-12.1	183
8[1]	-30.2	-13.6	287
16[1]	-26.2	-13.2	288
16[2]	-25.2	-12	382

[1] 64 samples per run; [2] 100 samples per run

Clearly, reconstruction performance deteriorates as the number of faults increases. For 8 faults the reconstructed array excitation error is less than -30dB, but this can be improved by increasing the number of samples per run from 36 to 64 and this is shown in Table II. This of course means that more NF samples need to be taken, 287 instead of 183 in this case. The last line of Table II shows the case for 16 faulty elements (2.9% array element failure rate). At 16 failed elements, the upper limit of sparsity is being approached and adding more samples does not improve performance as shown in the last row of Table II where 100 samples per run are used and the overall performances measures are marginally worse. The performance metrics described above have concentrated on the recovered amplitude of the reconstructed array excitation, however, and as can be seen from Figure 3 the phase is also

well recovered with an RMS phase error over the whole array of 2.6° with a maximum error of 51°. The high maximum is a function of the fact that one of the set element amplitude errors is -30 dB and so reconstruction the phase from such a small signal is always problematic. The ability to reconstruct the phase is exemplified by reconstructing an array that has a beam scan of 20° in azimuth and 10° in elevation applied to it, where the performance in amplitude is shown in Table I and the reconstructed phase is shown in Figure 7. The performance difference between scanned and not scanned case is small, with the scanned case being slightly better (recovered rms phase error over the whole array of 2.3° with a maximum error of 40.8°).

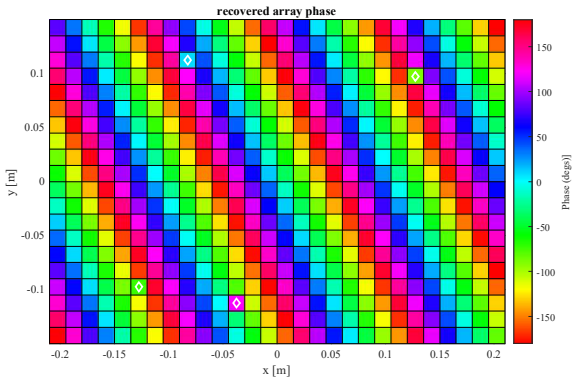

Figure 7. Reconstructed phase for case of 20° azimuth and 10° elevation beam scanned array with all other parameters as in Figure 3.

V. Conclusions

This early-stage investigation of array diagnostics using NF CS has provided a strong indication of the levels of performance that can be achieved using conventional convex optimisation-based CS are similar to those achieved for the FF sampled case [1]. So -30dB MSE measurement to element ratio (M/N) of <0.33. There is a clear limit to the array element failure rate (about 2%) before this approach begins to produce poor reconstruction performance. In [17] the Bayesian Compressive Sensing (BCS) framework was applied to this 'gold' array comparison approach, the work demonstrated that diagnostic errors of order -30dB (are achievable with FF measurement to element ratio (M/N) of >0.6. BCS is also more complicated to use, requiring several control parameters to choose before use. However, [16] demonstrates that a much higher failure rates (up to 32%) can be achieved with MSE better than -20dB, but at the expense of much higher sampling rate. In our future work we will be comparing and contrasting these two methods for production testing and examining the circumstances when failure rates will be acceptably small.

References

[1] S.F. Gregson, Z. Qin, C.G. Parini, "Compressive Sensing in Massive MIMO Array Testing: A Practical Guide", IEEE Transactions on Antennas and Propagation, 2022, Volume: 70, Issue: 9

[2] Wonil Roh, "5G Mobile Communications for 2020 and Beyond - Vision and Key Enabling Technologies," *IEEE WCNC 2014 Keynote*, Apr. 2014.

[3] Z. Pi and F. Khan, "An introduction to millimeter-wave mobile broadband systems," *IEEE Commun. Mag.*, vol. 49, no. 6, pp. 101–107, Jun. 2011.

[4] C. G. Parini, S. F. Gregson, J. McCormick, D. Janse van Rensburg "Theory and Practice of Modern Antenna Range Measurements", *IET Press,* 2014, ISBN 978-1-84919-560-7. (second edition published in 2021)

[5] D.L. Donoho, "Compressed sensing," in *IEEE Trans. Inf. Theory*, vol. 52, no. 4, Apr. 2006

[6] R. Cornelius, D. Heberling, N. Koep, A. Behboodi and R. Mathar, "Compressed sensing applied to spherical near-field to far-field transformation," in *Proc. European Conf. Antennas Propag. (EuCAP),* Davos, Switzerland, 2016, pp. 1-4.

[7] C. Culotta-López and D. Heberling, "Fast spherical near-field measurements on arbitrary surfaces by application of pointwise probe correction to compressed sampling Schemes," *in Proc. Antenna Measurement Techniques Association Symposium (AMTA),* San Diego, CA, USA, 2019, pp. 1-6

[8] M. Salucci, M. D. Migliore, P. Rocca, A. Polo and A. Massa, "Reliable antenna measurements in a near-field cylindrical setup with a sparsity promoting approach," *IEEE Trans. Antennas Propag.*, vol. 68, no. 5, pp. 4143-4148, May 2020

[9] M. D. Migliore, "A compressed sensing approach for array diagnosis from a small set of near-field measurements," *IEEE Trans. Antennas Propag.*, vol. 59, no. 6, pp. 2127–2133, Jun. 2011.

[10] B. Fuchs and M. D. Migliore, "Array diagnosis from far field data via ℓ1 minimizations," *Proc. European Conf. Antennas Propag. (EuCAP),* The Hague, Netherlands, 2014, pp. 1239-1242

[11] B. Fuchs, L. L. Coq, and M. D. Migliore, "Fast antenna array diagnosis from a small number of far-field measurements," *IEEE Trans. Antennas Propag.*, vol. 64, no. 6, pp. 2227–2235, Jun. 2016.

[12] S.F. Gregson, J. McCormick, C.G. Parini, "Principles of Planar Near-Field Antenna Measurements 2nd Edition", IET Press, Sept. 2023.

[13] C.C. Paige, M.A. Saunders, "LSQR: An Algorithm for Sparse Linear Equations and Sparse Least Squares", ACM Transactions on Mathematical Software, Vol. 8, No. 1, March 1982, pp. 43–71.

[14] Michael Grant and Stephen Boyd. CVX: Matlab software for disciplined convex programming, version 2.0 beta. http://cvxr.com/cvx, September 2013.

[15] E.J. Candes, M. B. Wakin,S. P. Boyd, "Enhancing sparsity by reweighted ℓ1 minimization", J. *Fourier Anal Appl 14*, pp. 877-905, 2008.

[16] Michael Grant and Stephen Boyd, "CVX: Matlab Software for Disciplined Convex Programming, Version 2.0 beta," http://cvxr.com/cvx, September 2013.

[17] M. Salucci, A. Gelmini, G. Oliveri and A. Massa, "Planar array diagnosis by means of an advanced Bayesian compressive processing," *IEEE Trans. Antennas Propagation*, vol. 66, no. 11, pp. 5892-5906, Nov.